SCA-9735

CORE ELASTIC PROPERTIES OF THE MONTEREY FORMATION, SANTA MARIA BASIN, CALIFORNIA

Xingzhou Liu, Texaco Exploration & Production Technology Department
Lev Vernik, ARCO Exploration & Production Technology Company
Robert A. Skopec, Texaco Exploration & Production Technology Department

Abstract

Monterey Formation core and outcrop samples were characterized to study the effects of lithology, sedimentology, and diagenesis on their elastic properties. Rock types present in the sample set are porcelanite, siliceous shale, shale, and dolomite. Factors that most strongly affect elastic wave velocities, using the ultrasonic transmission technique, are the relative volume proportions of dolomite and kerogen-rich detritus, followed by porosity, texture (laminations), effective pressure, and fluid saturation. For sonic porosity interpretation, four lithology groups were identified: a) dolomite; b) silty dolomite; c) chert, porcelanite and dolomitic shale; and d) kerogen-rich shales. Strong elastic anisotropy was found in phosphatic shale consisting of alternating cryptocrystalline phosphate and kerogen-rich clay laminae, as well as outcrop porcelanite that is highly laminated, but much less compacted than its core counterpart. Compaction induced porosity reduction of about 30% was observed between core and outcrop samples. Permeability anisotropy is much higher than that of the velocity. Results from this study can be used in sonic log and seismic interpretations.

Introduction

The Miocene Monterey Formation is a principal petroleum source rock and in many fields an important reservoir rock in both onshore and offshore southern California[3]. Its petrophysical properties are complex because of large variations in mineral composition and porosity, strong layering, and the presence of fractures arising from sedimentology, diagenesis, and post-depositional tectonics. In well logs, dolomites typically exhibit high density and low gamma ray count in contrast to shales that are easily distinguished. However, siliceous rocks, i.e., chert, porcelanite, and siliceous shales, are rather 'featureless' in all logs. Thickness of these layers is typically one- to two feet, often below the resolution of many wireline tools because of tool averaging effects. In addition, extensive fractures in thinly layered brittle rocks further complicates sonic log interpretation. In measuring porosity from sonic travel time, one cannot assume constant matrix travel time and a single shale volume correction across all lithologies. The primary goal of this work was to experimentally measure the elastic properties of all representative lithologies in the Monterey Formation and understand how sedimentology, diagenesis, and tectonics affect porosity estimations.

Methodology

Sample selection and preparation

Since the Monterey Formation rocks are very heterogeneous, two to three one half foot-long core pieces that were homogeneous over the interval were sampled for each representative lithology from core descriptions[1] and well logs. Outcrop samples were used to extend the high porosity/low compaction data range. For velocity measurements, three cylindrical plugs were drilled out of each core piece next to each other along three directions: parallel, normal and forty-five degrees to the bedding direction. The plugs were one inch in diameter, one to one and a half inches long, and plug ends were carefully polished to be smooth and parallel to allow good transducer contact and propagation of elastic waves along the axial direction of plugs.

Mineralogy, lithology and texture determination

Lithology and rock type were inferred from XRD mineralogy and core lithology descriptions. Following MacKinnon[6], ternary diagrams with end members of silica, detritus, and dolomite were used. The shale group was subdivided into siliceous shale, phosphatic shale and organic shale depending on the relative richness in silica, phosphate, and kerogen (see Figure 1). Texture at the millimeter and sub-millimeter scales was obtained from thin-section transmission light petrographic studies with magnifications of 40 to 200X. The most significant textural feature of the sample set (except sample 4590) was the intensity of laminations at fine scales. For example, in porcelanite (samples 4560 and 4571), the laminae consist of dark clayey bitumen and siliceous material. In phosphatic shale and dolomite, the siliceous material was replaced by phosphate and dolomite appeared as either carapace fragments or individual grains. The laminae spacing ranged from the order 0.01 *mm* to 1 *mm*. Sample petrophysical and mineralogical properties are listed in Table 1 of the Appenidx.

Porosity and density measurements

Both helium expansion and water saturation methods were used to measure samples' porosities and calculate their matrix densities. All three plugs from each core piece were used and the results were averaged. To ensure homogeneity, the densities of three plugs should not differ by more than 0.2 g/cm^3 and the porosity difference, as defined by $Df/f_{average}$, should be less than 15%. Samples that did not meet our criteria were not used for elastic measurements.

Liquid permeability measurement

Because shales are very impermeable, only a few high porosity outcrop samples were evaluated. Permeability was measured using a steady-state water flow technique at room temperature and calculated by the Darcy's law[7]. The confining pressure used was 10 *MPa* and the differential pressure along sample length was 2 *MPa*. Each measurement took about three hours to reach steady flow. Error in permeability measurement was estimated to be less than 2%. Table 2 lists the measurement results from 4 samples.

Measurement of elastic properties of rocks

The ultrasonic pulse transmission technique was used to measure elastic wave velocities from pulse travel times as defined by first break wave signatures and sample length. Pulse central frequencies for P-wave is 1 *MHz* and for S-wave 500 *kHz*. Velocity measurement accuracy using this technique is about 1% for P-wave and 2% for S-wave velocities. Measurements were made under both dry and brine saturated conditions in the effective pressure range of 5 to 50 *MPa* for outcrop samples and 5 to 40 *MPa* for core. Velocities measured along three directions and densities were then used to calculate the elastic stiffness tensor elements and anisotropy parameters (Appendix A). Because of uniform layering over the sample scale, transversely isotropic symmetry was assumed so that only five independent elastic constants were needed. Transverse anisotropy parameters, e and g, were used to represent P-wave and SH- or SV-wave anisotropy. Additional anisotropy parameters, d and d_{sv}, introduced by Thomsen[9] and Vernik et. al.[10] were also calculated to approximate P- and SV-wave velocities for close-to-normal direction wave velocities.

Results and discussion

Pressure effect

Ultrasonic velocities were measured in the effective confining pressure range of 2 to 40 *MPa* for core and 5 to 50 *MPa* for outcrop samples (saturated sample data are given in Table 3). Effective pressure is known to increase elastic wave velocities in rocks from microcrack closure and inter-particle contact strengthening in igneous rocks, limestone, and clay-free sandstones and, additionally, re-arrangement of clay particles in shales. Pore space compressibility is usually a secondary effect. Microcrack closure and grain contact often leads to flattening of velocites at a pressure range of 40 to 80 *MPa*. This was the case with sample 4590 which was a dense and almost pure dolomite (93.4%) and brittle porcelanite samples 4560 and 4571. Particle re-arrangement on the other hand leads to a continuous increase in velocity even beyond the high pressure end that corresponds to the estimated overburden stress of most sedimentary basins; this was observed in all other clay-rich samples. The largest velocity variation was observed in siliceous dolomite, i.e., samples 4642 and 4771, which had abundant dolomite particles in partial contact immersed in a ‘soft’ kerogen-clay matrix. When pressure was increased, the number of contacts among these ‘hard’ grains was increased, which caused velocities to increase rapidly.

Saturation effect

There are at least three ways that saturating fluids change elastic wave velocities of rocks: 1) pore stiffening; 2) physical weakening (lubrication); 3) chemical weakening; and 4) dispersion. The following expressions of Gassman’s relations can be used to show how elastic properties of saturated rocks (denoted by subscript ‘sat’) are related to the properties of dry rock (denoted by ‘dry’), matrix (denoted by ‘o’), as well as porosity.

$$K_{sat} = (1 + a_g) K_{dry}$$

$$G_{sat} = G_{dry}$$

$$r_{sat} = r_o (1 - f) + r_{fluid} f$$

$$a_g = \frac{\frac{K_o}{K_{dry}} + \frac{K_{dry}}{K_o} - 2}{f(\frac{K_o}{K_{fluid}} - 1) + (1 - \frac{K_{dry}}{K_o})}$$

It can be seen that the softer the rock (i.e., lower K_{dry}/K_o ratio) and/or the higher the porosity, the greater is the change in bulk modulus. This explained why samples 4696, 2, 3, 5, and 7 had the greatest variation in velocity with saturation. The chemical weakening effect was not very significant in the Monterey Formation as the clay type was mainly illite. It was estimated[5] that utlrasonic frequency used here was much lower than the Biot critical frequency and therefore dispersion correction was not necessary.

Effects of mineralogy and porosity

From the velocity-porosity plot in Figure 2, we found four distinct lithology groups: dolomite, silty dolomite, porcelanite, and shales. Extrapolating these regression lines we should be able to get the approximate average matrix velocities of these lithology groups. Modeling of the matrix velocities from lithology confirms the validity of this division (see Figure 1, right). Since dolomite and kerogen rich shale are the high and low velocity members of the velocity ternary diagram, the relative volume proportions of these two components control the matrix velocities of the matrix. Silica rich lithology has the intermediate matrix velocity, therefore it is difficult to distinguish chert, porcelanite, and highly siliceous shale from dolomitic shales by the sonic log alone. For porosity estimation from sonic logs, however, the above velocity-porosity relations have to be corrected for porosity-reduction with pressure.

Direction variation - anisotropy

Strong interlayering of different lithologies on the foot scale and lamination of different mineral components at the millimeter to sub-millimeter scale were one of the most significant characteristics of the Monterey Formation. The layering should cause strong directional dependence in seismic and sonic wave propagation velocities. At the ultrasonic wavelength scale, micro-lamination are more important. Except sample 4590 which had very low anisotropy because of the massive nature of this almost pure dolomite, all other samples demonstrated some degree of anisotropy (see Figure 3). Brittle rocks, i.e., porcelanite and siliceous shales had lower anisotropy than the others. The highest anisotropy was observed in sample 4696 (phosphatic-organic shale) which consists of an alternating phosphate and clay mixture, and has the highest kerogen content. In the outcrop samples, the highest anisotropy was observed in porcelanite and shales demonstrating the effect of lesser compaction on elastic anisotropy.

Fracture effect

The three major sets of fractures in the Monterey Formation are nearly vertical, one parallel, one perpendicular, and one forming 45^o to the anticlinal axis. Since our plugs were too small to sample these fractures, the matrix properties studied here may be used as the intact rock properties to model the effect of fracture sets for the sonic and seismic measurements[5].

Conclusions

Laboratory measurements of the petrophysical properties of the Monterey Formation core and outcrop samples showed that mineral composition, porosity, confining pressure, fluid saturation and wave propagation direction had the strongest effects on the elastic properties. For sonic log porosity calculation, the following steps are suggested: 1) identify lithology, 2) estimate net reservoir pressure, 3) correct for the directional dependence of sonic velocity, and 4) correct for any fluid substitution effect. From sonic log-core comparison[4], it was found that velocities agree better in softer shales than in brittle rocks, implicating the effect of fractures on sonic measurement. If confirmed by fracture analysis from the same well, the velocity discrepancy between core and in situ measurements can be used for fracture detection. The micro-Darcy permeability of the high porosity outcrop sample varies with fluid flow direction. The anisotropy ratio (10:1, higher in bedding parallel direction) is much higher than the velocity anisotropy ratio (2:1) for the same sample at the same confining pressure (10 MPa).

Acknowledgments

Core samples in this study were kindly provided by Unocal. Permeability measurement was made at USGS (Menlo Park). Help from Dr. C. Morrow was greatly appreciated. This work was funded by an industrial consortium of oil companies, including Arco, BP, Mobil, Marathon, Norsk Hydro, Shell, Texaco and Unocal, through Stanford University. The authors want to thank management of TEXACO and ARCO for permission to publish this paper.

Nomenclature

symbols

f	= porosity	K, G	= bulk and shear moduli
V_P	= P-wave velocity	C_{ij}	= elastic stiffness elements
$V_{SH, SV}$	= S-wave velocities	e, g, d, d_{sv}	= anisotropy parameters

unit conversions

1 MPa = 10^6 Pa; 1 Pa = 0.000145 psi

1 km/s = 3281 ft/s

References

[1] Dunham, J. B., and Cotton-Thornton, M. L., “Lithology of the Monterey Formation in the western Santa Maria valley field, Santa Maria basin, California”, SEPM Core Workshop 14, (1990), 203-239.

[2] Gassmann, F., “Uber die elastizitat poroser medien”, *Vier. der Natur Gesellschaft* 1951 (96), 1-23.

[3] Isaacs, C. M., “Field characterization of rocks in the Monterey Formation along the coast near Santa Barbara, California”, in AAPG Field Guide 4, 1981, 9-24.

[4] Liu, X., “Nonlinear elasticity, seismic anisotropy, and petrophysical properties of reservoir rocks”, Ph.D. thesis, Stanford University (1994).

[5] Liu, X., Vernik, L., and Nur, A., “Effects of saturating fluids on seismic velocities in shales”, in Expanded Abstr. 63rd Ann. Internat. Mtg. Soc. Expl. Geophys., (1995).

[6] MacKinnon, T. C., “Petroleum geology of the Monterey Formation in the Santa Maria and Santa Barbara coastal and offshore area”, in Coal and hydrocarbon resources of North America, v.1. Oil in the California Monterey Formation, ed. by MacKinnon, T. C., 1989.

[7] Morrow, C. A., and Byerlee, J. D., “Permeability of core samples from Cajon Pass scientific drillhole: Results from 2100 to 3500 m depth”, J. Geophys. Res., (1992) 97(B3), 5145-5151.

[8] Sadler, R. K., “The relationship of lithology and tectonics to fracturing in the Monterey Formation, Point Arguello field, offshore California”, SEPM Core Workshop 14, (1990), 245-269.

[9] Thomsen, L., “Weak elastic anisotropy”, Geophysics, (1986) 51, 1954-1966.

[10] Vernik, L., and Nur, A., “Ultrasonic velocity and anisotropy of hydrocarbon source-rocks”, Geophysics, (1992) 57, 727-735.

Table 1. Sample petrophysical and petrochemical properties (*por*-porosity at atmospheric pressure, *b.den*-bulk density in dry condition, *m.den*-matrix density calculated from *por* and *b.den*, *ker*-kerogen, *TOC*-total organic content, *dolo*-dolomite, *detri*-detritus, *sili.dolom*-siliceous dolomite, *sili. shale*-siliceous shale)

sample No.	*depth (m)*	*por (%)*	*b.den (g/cm^3) (dry)*	*m.den (g/cm^3)*	*ker (%) (vol)*	*TOC (%) (wt)*	*dolo (%) (vol)*	*detri (%) (vol)*	*silica (%) (vol)*	*lithology*
core										
4560	1390	11.4	1.92	2.17	0.058	2.40	0.0	20.8	73.2	porcelanite
4571	1393	10.0	1.93	2.14	0.055	2.28	0.0	15.1	79.0	porcelanite
4590	1399	3.0	2.64	2.72	0.006	0.19	93.4	2.3	0.0	dolomite
4642	1415	16.5	1.99	2.38	0.202	8.12	64.6	24.6	0.0	sili. dolom
4685	1428	21.0	1.86	2.35	0.190	8.19	35.5	40.7	0.0	shale
4696	1431	21.0	1.60	2.02	0.363	18.2	0.0	61.2	0.0	shale
4771	1454	19.0	2.02	2.49	0.147	5.83	59.2	19.1	0.0	sili. dolom
4798	1462	18.0	1.93	2.35	0.224	9.31	27.1	52.8	0.0	shale
5478	1670	4.3	2.14	2.24	0.182	6.81	0.0	84.4	0.0	sili. shale
5553	1692	11.0	2.40	2.70	0.016	0.52	64.2	29.6	0.0	sili. dolom
outcrop										
1	0	16.6	2.15	2.58	0.020					porcelanite
2	0	28.8	1.56	2.19	0.155	7.93				shale
3	0	30.9	1.44	2.08	0.280	15.6				shale
5	0	29.6	1.56	2.22	0.048	2.47				porcelanite
6	0	10.3	2.23	2.49	0.030	3.61				sili. shale
7	0	29.3	1.66	2.35	0.087	4.18				shale
8	0	5.9	2.56	2.72	0.051	1.60				sili. dolom
9	0	5.0	2.60	2.73	0.044	1.36				sili. dolom

Table 2. Liquid (water) permeability of selected outcrop samples (bedding normal is defined as 0 degree) measured at room temperature

sample No.	*direction (degrees)*	*liquid permeability (mDarcy)*
1	90	1.41
2	0	0.28
	90	2.52
3	90	6.94
5	90	3.67

Table 3. Ultrasonic velocities under confining pressures (brine-saturated)

sample No.	*Pc (MPa)*	*$V_P(0^o)$ (km/s)*	*$V_P(45^o)$ (km/s)*	*$Vp(90^o)$ (km/s)*	*$Vs(0^o)$ (km/s)*	*$Vs(45^oH)$ (km/s)*	*$Vs(90^o)$ (km/s)*	*$Vs(45^oV)$ (km/s)*
4560	2	3.82	3.79	4.12	2.48	2.45	2.56	2.42
	5	3.84	3.81	4.15	2.50	2.48	2.58	2.45
	10	3.86	3.83	4.17	2.51	2.50	2.60	2.48
	20	3.88	3.85	4.20	2.52	2.53	2.62	2.51
	30	3.90	3.87	4.21	2.54	2.56	2.63	2.53
	40	3.91	3.89	4.23	2.55	2.58	2.64	2.54
4571	2	3.70	3.76	3.85	2.44	2.47	2.53	2.44
	5	3.71	3.77	3.86	2.45	2.48	2.54	2.45
	10	3.72	3.78	3.87	2.46	2.49	2.55	2.46
	20	3.74	3.80	3.88	2.47	2.51	2.57	2.48
	30	3.75	3.81	3.88	2.48	2.52	2.58	2.49
	40	3.76	3.82	3.89	2.49	2.53	2.59	2.50
4590	2	5.95	5.75	6.72	3.50	3.36	3.71	3.29
	5	6.03	5.85	6.76	3.52	3.39	3.72	3.32
	10	6.10	5.95	6.81	3.54	3.43	3.73	3.37
	20	6.17	6.05	6.87	3.57	3.47	3.75	3.41
	30	6.23	6.11	6.92	3.60	3.49	3.77	3.44
	40	6.29	6.17	6.97	3.62	3.52	3.78	3.46
4642	2	2.89	3.05	3.52	1.90	2.02	2.20	1.81
	5	3.02	3.13	3.55	1.95	2.05	2.22	1.88
	10	3.12	3.22	3.60	1.99	2.08	2.24	1.93
	20	3.25	3.33	3.68	2.04	2.13	2.27	2.00
	30	3.37	3.44	3.75	2.08	2.17	2.30	2.04
	40	3.45	3.53	3.83	2.12	2.21	2.33	2.08
4685	2	1.82		2.94	1.46		1.76	
	5	1.91		2.98	1.49		1.78	
	10	2.05		3.03	1.52		1.81	
	20	2.32		3.12	1.60		1.86	
	30	2.52		3.22	1.66		1.90	
	40	2.68		3.28	1.72		1.94	
4696	2	2.02	2.46	3.22	1.43	1.78	2.05	1.49
	5	2.13	2.55	3.26	1.45	1.80	2.06	1.53
	10	2.25	2.65	3.29	1.48	1.82	2.07	1.56
	20	2.37	2.76	3.31	1.52	1.84	2.08	1.59
	30	2.49	2.84	3.34	1.55	1.86	2.09	1.62
	40	2.56	2.89	3.36	1.58	1.88	2.10	1.65
4771	2	2.42	2.78	3.24	1.67	1.84	1.96	1.77
	5	2.51	2.84	3.28	1.70	1.87	1.98	1.80
	10	2.59	2.91	3.35	1.74	1.90	2.01	1.84
	20	2.77	3.05	3.45	1.80	1.95	2.06	1.90
	30	2.90	3.16	3.56	1.84	2.00	2.10	1.96
	40	3.01	3.24	3.64	1.91	2.04	2.14	2.01
4798	2	2.20	2.64	3.20	1.66	1.78	1.93	1.67
	5	2.38	2.71	3.23	1.72	1.81	1.95	1.72
	10	2.50	2.81	3.26	1.77	1.85	1.97	1.76
	20	2.67	2.92	3.30	1.83	1.90	2.00	1.82
	30	2.77	2.99	3.33	1.87	1.94	2.02	1.86
	40	2.85	3.04	3.37	1.90	1.97	2.04	1.90
5478	2	3.60	3.69	4.06	2.35	3.69	2.60	2.31

	5	3.62	3.71	4.07	2.36	3.71	2.61	2.33
	10	3.64	3.74	4.08	2.38	3.74	2.62	2.35
	20	3.66	3.77	4.10	2.39	3.77	2.63	2.36
	30	3.68	3.79	4.11	2.40	3.79	2.64	2.37
	40	3.70	3.82	4.12	2.41	3.82	2.65	2.38
5553	2	4.57		5.32	2.84		3.32	
	5	4.66		5.34	2.85		3.33	
	10	4.73		5.37	2.89		3.34	
	20	4.83		5.40	2.93		3.36	
	30	4.93		5.43	2.96		3.37	
	40	5.03		5.46	3.00		3.38	
1	5	3.60	3.70	4.28	2.03	2.08	2.16	1.95
	10	3.64	3.75	4.31	2.05	2.10	2.17	1.98
	20	3.69	3.80	4.34	2.07	2.12	2.18	2.00
	30	3.74	3.85	4.36	2.08	2.13	2.19	2.01
	50	3.82	3.91	4.39	2.11	2.16	2.20	2.04
2	5	2.52	2.56	2.72	1.33	1.36	1.41	1.28
	10	2.56	2.60	2.75	1.34	1.37	1.42	1.30
	20	2.61	2.65	2.80	1.36	1.38	1.44	1.31
	30	2.65	2.69	2.84	1.37	1.39	1.45	1.32
	50	2.71	2.75	2.89	1.39	1.41	1.47	1.36
3	5	2.12	2.10	2.23	1.14	1.24	1.36	1.16
	10	2.20	2.16	2.30	1.15	1.25	1.39	1.17
	20	2.28	2.24	2.38	1.17	1.27	1.41	1.18
	30	2.36	2.33	2.47	1.20	1.29	1.43	1.21
	50	2.48	2.45	2.58	1.24	1.31	1.46	1.24
5	5	2.60	2.74	3.06	1.38	1.46	1.77	1.48
	10	2.62	2.77	3.08	1.39	1.47	1.78	1.50
	20	2.66	2.81	3.10	1.40	1.48	1.79	1.52
	30	2.70	2.85	3.13	1.41	1.50	1.80	1.53
	50	2.74	2.88	3.15	1.42	1.52	1.81	1.55
6	5	4.34	4.43	4.63	2.52	2.54	2.69	2.52
	10	4.37	4.46	4.66	2.53	2.55	2.70	2.54
	20	4.41	4.49	4.70	2.55	2.56	2.72	2.56
	30	4.44	4.52	4.73	2.56	2.57	2.73	2.57
	50	4.48	4.56	4.77	2.58	2.59	2.75	2.59
7	5	2.42	2.57	2.68	1.22	1.33	1.43	1.30
	10	2.48	2.62	2.72	1.24	1.35	1.44	1.31
	20	2.54	2.67	2.77	1.27	1.37	1.46	1.33
	30	2.60	2.71	2.81	1.29	1.40	1.47	1.34
	50	2.66	2.77	2.88	1.32	1.42	1.49	1.35
8	5	4.66	4.82	5.20	2.58	2.65	2.78	2.57
	10	4.72	4.87	5.24	2.61	2.67	2.80	2.60
	20	4.83	4.95	5.28	2.64	2.70	2.82	2.63
	30	4.91	5.01	5.32	2.67	2.73	2.84	2.66
	50	5.03	5.12	5.40	2.72	2.78	2.87	2.72
9	5	4.68	4.95	5.17	2.59	2.70	2.77	2.65
	10	4.75	5.02	5.23	2.62	2.73	2.80	2.69
	20	4.86	5.11	5.31	2.66	2.77	2.83	2.73
	30	4.93	5.17	5.38	2.69	2.80	2.85	2.76
	50	5.00	5.25	5.46	2.73	2.84	2.89	2.81

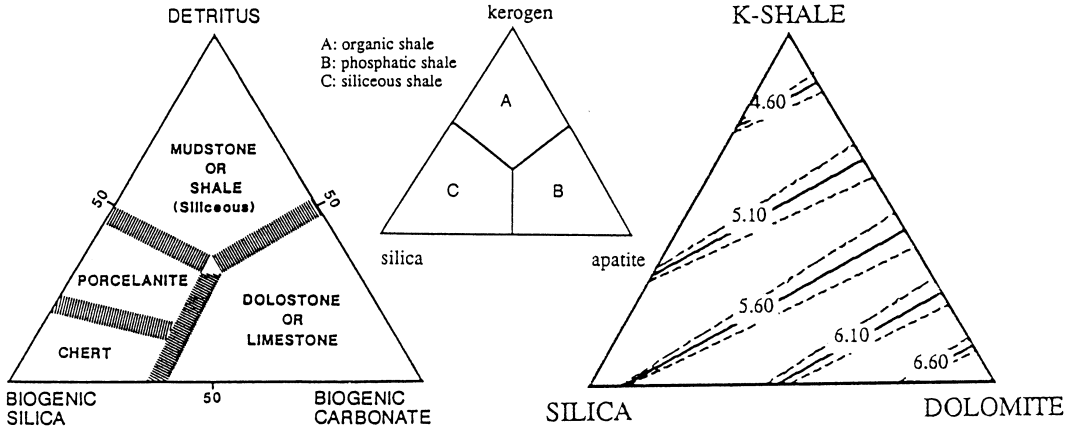

Figure 1. Left: Ternary diagrams of major rocks types in the Monterey Formation: siliceous rocks (chert, porcelanite), shale, and dolomite (after MacKinnon, 1989); middle: subdivision of shale into organic, sliceous, and phosphatic shales; right: modeling result of rock matrix P-wave velocities (unit: km/s) plotted in the same ternary diagram.

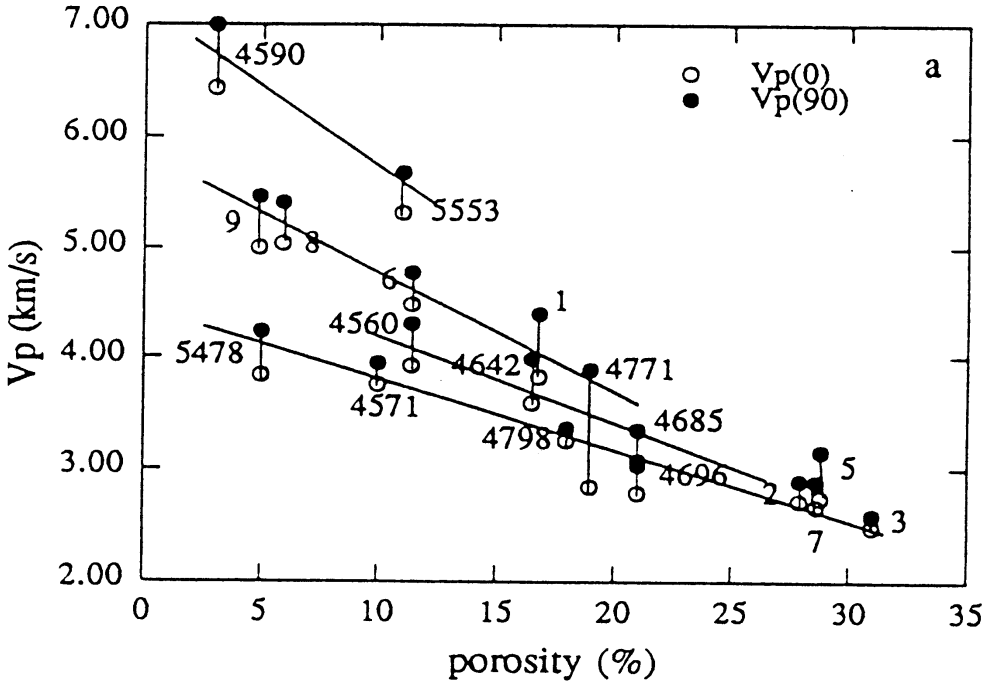

Figure 2. Laboratory measured ultrasonic velocities at the confining pressure of 40 *MPa* versus porosity (lab condition). Four lithology groups can be identified from the plot: dolomite, silty dolomite, siliceous rocks (porcelanite), and kerogen-rich shales. Extrapolated matrix P-wave velocities for the four groups are 7.16, 5.90, 5.12, 4.37 km/sec respectively. Correction of porosity-reduction at high pressure should be made when using the linear correlation relations.

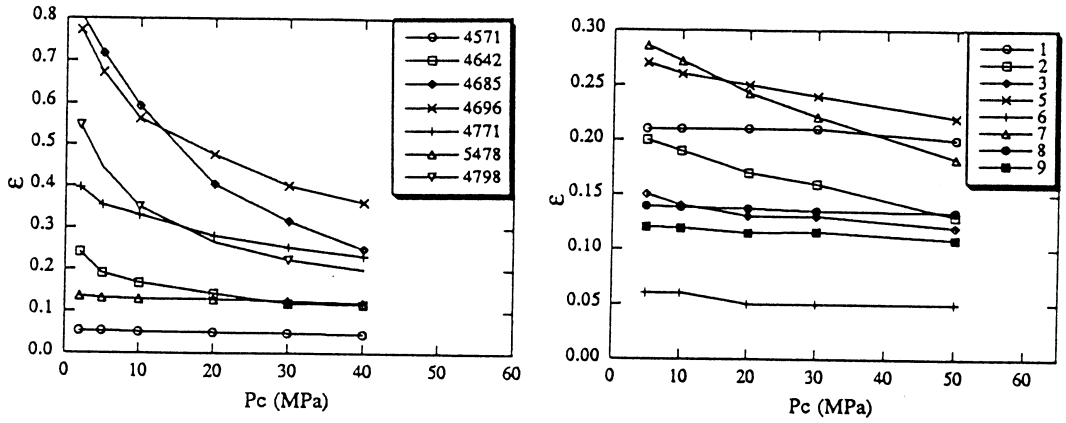

Figure 3. Measured elastic anisotropy parameter, *e*, versus confining pressure Pc (in MPa) for Monterey Formation rock samples (left: core; right: outcrop).

Appendix

Relationships between elastic stillness tensor (C_{ij}) and velocities along symmetry axis V(0^o), 45^o relative to symmetry axis V(45^o) and perpendicular to symmetry axis V(90^o) and relationships between anisotropy parameters (e, g, d and d_{SV}) and elastic constants (both for transversely isotropic materials)

$$C_{11} = rV_P{}^2(90^o)$$
$$C_{12} = C_{11} - 2rV_{SH}{}^2(90^o)$$
$$C_{33} = rV_P{}^2(0^o)$$
$$C_{44} = rV_{SH}{}^2(0^o)$$
$$C_{13} = -C_{44} + \sqrt{4r^2V_P{}^4(45^o) - 2rV_P{}^2(45^o)(C_{11} + C_{33} + 2C_{44}) + (C_{11} + C_{44})(C_{33} + C_{44})}$$
$$C_{66} = rV_{SH}{}^2(90^o)$$

$$e = (C_{11} - C_{33}) \Big/ (2C_{33})$$
$$g = (C_{66} - C_{44}) \Big/ (2C_{44})$$
$$d = \frac{(C_{13} + C_{44})^2 - (C_{33} - C_{44})^2}{2C_{33}(C_{33} - C_{44})}$$
$$d_{SV} = \frac{(C_{11} - C_{44})(C_{33} - C_{44}) - (C_{13} + C_{44})^2}{2C_{44}(C_{33} - C_{44})}$$